Available online at www.sciencedirect.com
SCIENCE DIRECT®
PERGAMON
Chaos, Solitons and Fractals 18 (2003) 1001–1014
CHAOS
SOLITONS & FRACTALS
www.elsevier.com/locate/chaos

Chaos in a bienzymatic cyclic model with two autocatalytic loops

H. Berry *

Equipe de Recherche sur les Relations Matrice Extracellulaire-Cellules (ERRMECe), Université de Cergy-Pontoise, 2 avenue A. Chauvin. B.P. 222, Cergy Pontoise Cedex 95302, France

Accepted 24 February 2003

Abstract

A general bienzymatic cyclic system including two autocatalytic loops is studied and used as a basic design principle for modelling extracellular matrix turnover. Using classical enzyme kinetic rates, the model is described by a set of four ordinary differential equations and numerically studied by bifurcation diagrams and Poincaré sections. We observe limit-cycle oscillations and chaotic behaviors arising from period-doubling cascades or intermittency. Chaotic oscillations originate from distinct strange attractors that undergo boundary and internal crisis. For some parameter values, the system presents several bistable areas, where a limit cycle coexists with another one or with a strange attractor. The dynamics are qualitatively modified when the weight of the autocatalytic loops on the system varies, resulting in the change in the number of attractors.

1. Introduction

A bienzymatic cycle consists of two enzyme reactions organized in an anti-parallel fashion, in which the substrate A of the first enzyme is transformed into a product B, that is, in turn, converted back into A by the second one. These metabolic organizations are widespread in some cell molecular processes, such as reversible covalent modifications. An important example of such mechanisms consists of phosphorylation/dephosphorylation events that are predominantly observed in signal transmission inside cells. Several theoretical models of cyclically-organized biological reactions have previously been studied. In the absence of regulation (feedback loops), the only dynamical behavior accessible is monostability, although switch-like properties can be observed through zero-order ultrasensitivity [1–3]. When self-regulation is included, bistability and limit cycle oscillations may be obtained [4–9], as well as more complex dynamics if several bienzymatic cycles are themselves organized in a cyclic fashion [10]. Many of the theoretical predictions of these models have been confirmed experimentally [11–13].

Recently, we proposed a bienzymatic cycle regulated by an autocatalytic positive feedback loop, for modelling extracellular matrix degradation balance [14]. This model evidenced bistability and limit-cycle oscillation dynamics. In the present paper, we introduce a second autocatalytic loop in this bienzymatic cycle. The resulting doubly-regulated cyclic model is used as a basic design principle for a model of extracellular matrix turnover that takes transglutaminase regulation by the surrounding cells into account.

The extracellular matrix is an insoluble, gel-like mesh of various structural and functional macromolecules that forms connective tissues and basement membranes in animals. It constitutes both a barrier separating organisms into tissue compartments and a substratum for cell adhesion [15]. Besides this structural role, the extracellular matrix is an essential regulator of cell physiology, predominantly implicated in morphogenesis, cell survival, cell cycle and migration

* Fax: +33-134-25-65-52.
E-mail address: hugues.berry@bio.u-cergy.fr (H. Berry).

0960-0779/03/$ - see front matter
doi:10.1016/S0960-0779(03)00070-5

and tumorigenesis [16,17]. During normal maintenance or pathological modifications, the extracellular matrix undergoes intense cell-controlled turnover, involving both extracellular matrix degradation and synthesis. Regulation of extracellular matrix mass-balance is involved in many physiological processes such as embryogenesis [18], immune cell activation [19], reproductive cycles [20], wound healing [21], or pathological ones such as tumor dissemination [22].

The main focus in this paper is on the oscillatory behaviors displayed by the modelled system, and the diversity of the accessible oscillation modes. In Section 2, we introduce the ordinary differential equations describing the model, and study it in Section 3 through bifurcation diagrams and Poincaré sections. The dynamics display chaotic behaviors, as well as bistability and hysteresis when periodic limit-cycle oscillations coexist with a chaotic attractor. Finally, Section 4 presents some conclusions.

2. The model

The enzymatic system studied consists of two cyclically-organized enzyme reactions (Fig. 1, inset) interconverting compounds A and B via two antagonist enzymes E_1 and E_2. Two autocatalytic loops are introduced through the influence of B on the activity of both enzymes. B increases the rate of its formation (positive feedback loop) as well as that of its consumption (positive forward loop). We illustrate this basic design principle in the case of extracellular matrix degradation balance (Fig. 1).

Unsoluble extracellular matrix proteins (m) are degraded by protein-cleaving enzymes called proteinases (p) into soluble proteolysis fragments (f) while these fragments can be cross-linked by transglutaminase (g) or other intermolecular protein-cross-linking enzyme to yield back new unsoluble extracellular matrix proteins m. Thus the two antagonist enzymes consist here of proteinases (p) and transglutaminases (g), that interconvert extracellular matrix proteins (m) and soluble proteolysis fragments (f). The autocatalytic loops are due to f influence on p and g synthesis rate by the surrounding cells. In vivo, cells identify the characteristics of the surrounding extracellular matrix using several membrane receptors that specifically recognize extracellular matrix elements. These receptors provide cells with

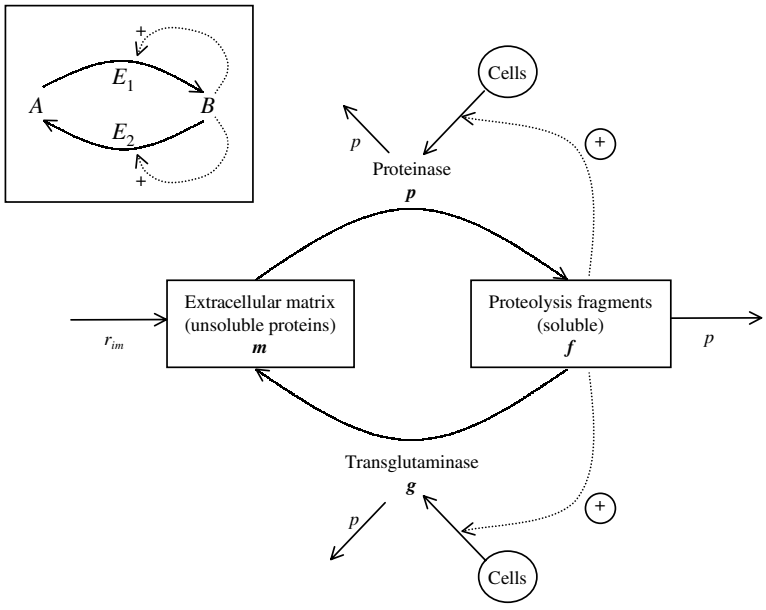

Fig. 1. Scheme of the bienzymatic cyclic model studied and exemplified in the case of extracellular matrix degradation balance. The inset shows the basic cyclic scheme. Two molecules A and B are interconverted by two antagonist enzymes (E_1 and E_2), forming a bienzymatic cycle. The compound B auto-catalytically increases the rate of its own formation and that of its consumption (autocatalytic loops, dashed arrows). This basic scheme is further implemented in the case of extracellular matrix degradation. Unsoluble extracellular matrix proteins (m) are produced by cells at constant rate r_{im} and degraded by proteinases (p) into soluble proteolysis fragments (f). Fragments can be cross-linked by transglutaminase (g) to yield back new unsoluble ECM proteins m. Fragments are subject to proteolysis from p and interact with cells to increase both proteinase and transglutaminase synthesis rates. Both enzymes undergo p-catalyzed proteolysis.

responses to extracellular matrix physical and chemical changes by modulating signal-transduction cascades into the cells [23,24]. For instance, in fibroblasts, proteolysis fragments of fibronectin (an extracellular matrix protein) induce expression and secretion into the extracellular matrix of neo-synthesized proteinases, whereas the entire fibronectin molecule does not [25]. Thus, f increases proteinase quantity, which, in turn increases f formation rate in a first autocatalytic loop. Similarly, transglutaminase expression and secretion by the cells can be regulated by the quantity of surrounding extracellular matrix [26]. We thus introduce a second autocatalytic loop, assuming the possibility of g up-regulation by the cells in response to f quantity. Besides the basic bienzymatic organization, other biologically-relevant processes must be taken into account. Extracellular matrix proteins m are produced by surrounding cells (taken here as a constant rate r_{im}). Moreover, each protein (whether m, f, g, or p) itself is subject to p-catalyzed degradation.

The equations describing this scheme (Eqs. (1)–(4)) are based on the classical Michaelis–Menten formalism [27] for every enzyme reaction, except for p autoproteolysis, which is modelled here as a simple second-order rate. Unlike most of the previously-published models of bienzymatic cycles, the autocatalytic loops do not act directly on enzyme activity, but control p and g cell-synthesis. We describe both autocatalytic loops as f-induced g or p cell-synthesis rates, r_g or r_p, respectively, and model them formally as sigmoid Hill-functions of f:

$$r_x = \frac{c_1 f^{n_{\mathrm{H}}}}{c_2^{n_{\mathrm{H}}} + f^{n_{\mathrm{H}}}}$$

where x is g or p. c_1 is the maximal rate (obtained for $f \gg c_2$) and represents the strength or level of the autocatalytic loop. c_2 is f concentration at half-maximal rate (often called ''threshold'' constant). The exponent n_{H} (Hill-number) controls the form of r_x: the higher n_{H}, the more r_x is a switch-like function of f. Note that cell quantity is assumed to be constant here, so that r_g and r_p only depend on f. A more detailed justification of the biological grounds as well as the form of the kinetic terms used in the equations can be found in [14].

m variation rate is described by Eq. (1):

$$\frac{\mathrm{d}m}{\mathrm{d}t} = k_g g \frac{f}{K_G + f} - k_p p \frac{m}{K_P + m} + r_{\mathrm{im}} \tag{1}$$

In the right-hand side of Eq. (1), the first term represents m production from f and g (with k_g and K_G, the corresponding catalytic and Michaelis constants, respectively), the second term is m consumption by proteolysis (with k_p and K_P, the corresponding catalytic and Michaelis constants, respectively), and the last one represents constant m synthesis by the cells. f variation is modelled by Eq. (2):

$$\frac{\mathrm{d}f}{\mathrm{d}t} = -k_g g \frac{f}{K_G + f} + k_p p \frac{m}{K_P + m} - k_p p \frac{f}{K_P + f} \tag{2}$$

The first two terms in this equation are identical to the corresponding terms in Eq. (1), and the last one represents f proteolysis by p, which is assumed, for simplicity, to occur with the same kinetic constants as m proteolysis. Eq. (3) describes p variation rate:

$$\frac{\mathrm{d}p}{\mathrm{d}t} = \alpha \frac{f^n}{K_R^n + f^n} - k_a p^2 \tag{3}$$

The first term in the right-hand side of Eq. (3) corresponds to the first autocatalytic loop (r_p), with α the level of this loop, K_R the threshold constant and n the Hill-number. The second term represents p autoproteolysis (second-order rate constant k_a). Eqs. (1)–(3) describe upregulation of proteinase synthesis by the fragments and is the model studied in [14]. In the present study, we add upregulation of transglutaminase concentration by surrounding cells:

$$\frac{\mathrm{d}g}{\mathrm{d}t} = \beta \frac{f^l}{K_S^l + f^l} - k_{\mathrm{deg}} p \frac{g}{K_{\mathrm{deg}} + g} \tag{4}$$

As in Eq. (3), the first term describes the second autocatalytic loop (r_g), with β as the level of the loop, K_S the threshold constant and l the Hill-number. The second term models transglutaminase (g) proteolysis as a Michaelis–Menten rate, with k_{deg} and K_{deg}, the corresponding catalytic and Michaelis constants, respectively.

We then non-dimensionalize the system (Eqs. (1)–(4)) by normalizing each variable (p, g, m and f) by K_P and time by $(1/k_p)$, and obtain the dimensionless system Eqs. (5)–(8):

$$\frac{\mathrm{d}m}{\mathrm{d}t} = k_g \frac{f g}{K_G + f} - \frac{m p}{1 + m} + r_{\mathrm{im}} \tag{5}$$

$$\frac{\mathrm{d}f}{\mathrm{d}t} = -k_g \frac{f\,g}{K_G + f} + \frac{m\,p}{1+m} - \frac{f\,p}{1+f} \tag{6}$$

$$\frac{\mathrm{d}p}{\mathrm{d}t} = \alpha \frac{f^n}{K_R^n + f^n} - k_a p^2 \tag{7}$$

$$\frac{\mathrm{d}g}{\mathrm{d}t} = \beta \frac{f^l}{K_S^l + f^l} - k_{\mathrm{deg}} \frac{g\,p}{K_{\mathrm{deg}} + g} \tag{8}$$

where concentrations (m, f, p, g, K_G, K_R, K_S and K_{deg}) are normalized by K_P; first-order rate constants (k_g and k_{deg}) are normalized by k_p; k_a by k_p/K_P; rates (r_{im}, α and β) by $k_p \times K_P$; and time by $(1/k_p)$.

Thanks to the adimensionalization, the system Eqs. (5)–(8) has two parameter less than the original dimensional one. Furthermore, realistic values for the parameters do not need to be known as absolute values, but only with respect to K_P and/or k_p. Examination of the available data in the literature allow to define realistic values for some of them [14]. Hence, in this paper, we fix (normalized values): $K_G = 0.1$; $K_{\mathrm{deg}} = 1.1$; $k_g = k_{\mathrm{deg}} = 0.05$, and $k_a = k_{\mathrm{deg}}/K_{\mathrm{deg}} = 0.0455$. Moreover, for simplicity, we set $n = l$. Note that m and f concentrations evolve under the action of existing enzymes, whereas p and g are brought into the system through cell synthesis. Thus we assume that the rates for enzyme synthesis are slower than m and f turnover rates. As a consequence, α and β will be smaller than the enzyme catalytic constants k_g and k_p.

We focus here on the case $K_R > K_S$, i.e. where the half-maximal rate for g synthesis by the cells is obtained for slightly lower f values than for p. Specifically, we set $K_R = 4.5$ and $K_S = 1$. Note however, that the dynamics described below can be observed with many other parameter values, i.e. in other parts of the parameter space. Finally, a limitation in the variation ranges of the parameters is implicitly contained in the use of the Michaelis–Menten formalism for enzyme rates, which is valid only for enzyme concentrations lower than the corresponding substrate [28]. In other words, the model is valid only for parameters yielding $m > p$, $f > g$ and $f > p$. Unfortunately, to our knowledge, valid kinetic expressions for enzyme rates do not exist outside this limitation.

3. Results

3.1. Low autocatalytic levels

We first study the case where maximal enzyme-synthesis rates (α and β) by the cells are low, i.e. where both autocatalytic influences of f are low. Fig. 2(A) shows for illustration p and g autocatalytic loop rates (r_p and r_g, respectively) for $\alpha = 0.026$ and $\beta = 7.5 \times 10^{-4}$. Whereas r_g is higher than r_p at low f values, r_p is higher for $f > 2$. Under these conditions, the dynamics of the system become chaotic for $n = l \geqslant 3$. Fig. 2 shows a projection in the m–f plane of the strange attractor (B) and the corresponding time-courses of f, p and g in Log-linear coordinates (C) for $n = l = 4$. The average "orbit" of the strange attractor, i.e. the time needed to cover one average "turn" over the attractor is long ($\approx 5 \times 10^3$ time units). The chaotic nature of the dynamics are first illustrated by the inspection of the power spectrum (Fig. 2(D)). The power spectrum is dense, with a great level of noise, which is generally a mark of chaotic behavior. Moreover, sensibility to initial conditions is apparent from the value of the maximal Lyapunov exponent, $\lambda_{\max}$. Maximal Lyapunov exponent were calculated according to [29]. For the strange attractor of Fig. 2(B), we obtain $\lambda_{\max} = (0.947 \pm 0.014) \times 10^{-4}$ bits/time unit. This value is low because the average orbital period is long, but is not zero. To compare with classical chaotic systems, it must be related to the duration of an average orbit. One then yields $\lambda_{\max} = 0.473 \pm 0.007$ bits/orbit. This value is of the same order than that obtained for the Rössler system ($\lambda_{\max} = 0.13$ bits/s or 0.78 bits/orbits), but lower than that of the Lorenz system ($\lambda_{\max} = 2.2$ bits/s or 1.36 bits/orbits) [29].

We further study the dynamics with bifurcation diagrams and Poincaré sections. Fig. 3 shows a bifurcation diagram with $\alpha = 0.026$, $\beta = 7.5 \times 10^{-4}$ and r_{im} as the bifurcation and parameter. For $r_{\mathrm{im}} < 7.7764 \times 10^{-3}$, the system possesses an unique stable fixed point that becomes unstable at $r_{\mathrm{im}} = 7.7764 \times 10^{-3}$ through a Hopf bifurcation. The evolution of the maxima of p with r_{im} in the resulting period-1 stable limit cycle are seen in the bifurcation diagram for $r_{\mathrm{im}} < 0.00909$. The dynamics go through a period-doubling cascade, yielding period-2^k limit cycles. The chaotic dynamics can then be studied with Poincaré sections. We compute these sections at maxima of p, i.e. we define Poincaré sections P as:

$$P = \{(m_i, f_i, g_i) \in \mathbb{R}^3 | \dot{p}_i = 0, \ddot{p}_i < 0\}$$

First-return maps of the sections are shown in Fig. 4 for increasing values of r_{im} in the chaotic region. The maps are all unidimensional, as expected for chaotic dynamics. At $r_{\mathrm{im}} = 0.00962$, i.e. just after the period-doubling accumulation

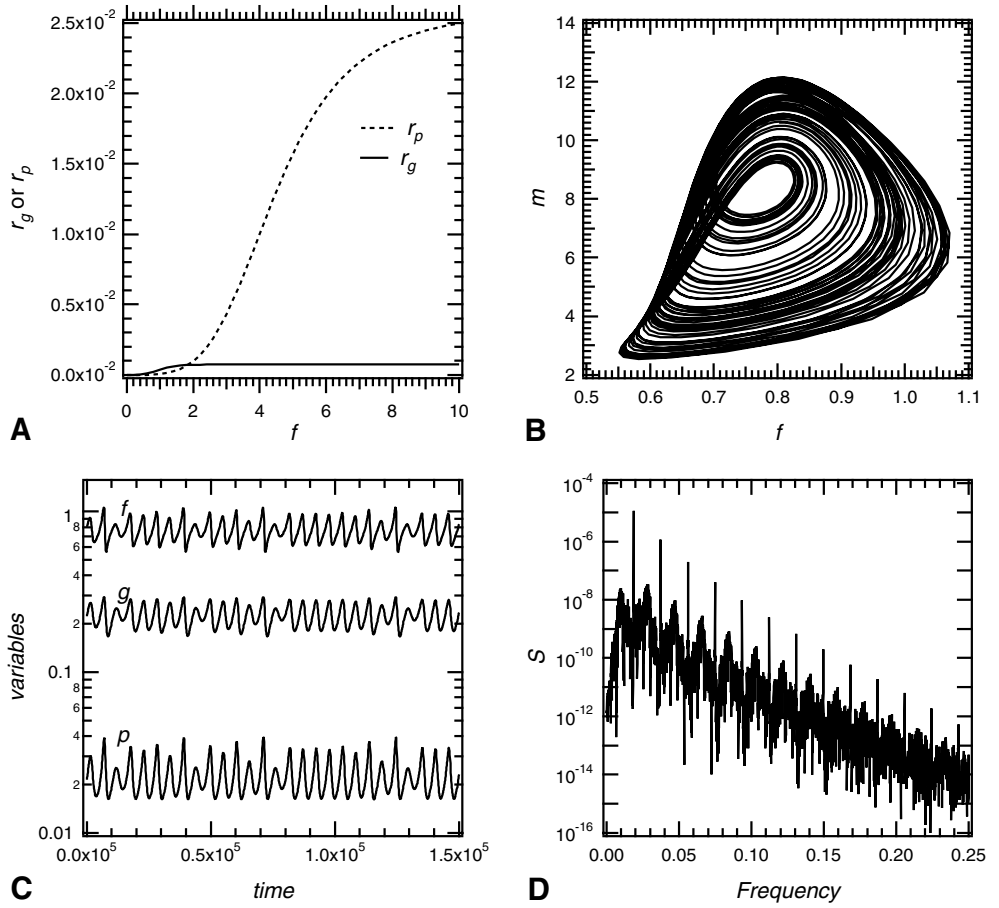

Fig. 2. (A) g (full line) and p (dashed line) cell-synthesis rates in response to f for $K_R = 4.5$, $K_S = 1$, $\alpha = 0.026$, $\beta = 7.5 \times 10^{-4}$ and $n = l = 4$. (B) Projection in the m–f plane of the strange attractor for the parameters of (A) and $K_G = 0.1$, $K_{\text{deg}} = 1.1$, $k_g = k_{\text{deg}} = 0.05$, $k_a = 0.0455$ and $r_{\text{im}} = 0.0098$. (C) Log-linear plot of f, g and p time-variations along the strange attractor of (B). (D) Log-linear plot of the corresponding power spectrum.

point, the map consists in four disjoint segments. This means that the chaotic oscillations are restrained in the neighborhood of a period-4 limit cycle. These first steps in the development of the chaotic dynamics are often called "noisy" orbits [30]. When r_{im} increases ($r_{\text{im}} = 0.00970$ in Fig. 4), two neighboring segments merge and the map forms a period-2 noisy orbit. This period-halving cascade goes on until the map becomes continuous ($r_{\text{im}} = 0.00980$ in Fig. 4).

The bifurcation diagram also shows that a saddle-node bifurcation occurs at $r_{\text{im}} = 0.00986$, giving rise to a stable and an unstable period-3 limit cycle (Fig. 3). Thus for $0.00986 \leqslant r_{\text{im}} \leqslant 0.00994$, the strange attractor coexists with the stable period-3 orbit, each one having its own basin of attraction. At $r_{\text{im}} = 0.00994$, the unstable period-3 limit cycle (plus signs in the bifurcation diagram) collides with the basin of attraction of the strange attractor. This collision abruptly destroys the strange attractor in a boundary crisis [31]. The coexistence of the strange attractor and the stable limit cycle is a cause of bistability and hysteresis in this region. This is exemplified in Fig. 5. At $r_{\text{im}} = 0.00985$, i.e. before the saddle-node bifurcation, the only stable element is the strange attractor so that the system settles down onto it. When r_{im} is then increased to 0.00990, the system remains on the strange attractor and the dynamics are chaotic (Fig. 5(A) and (C)). If r_{im} is further increased beyond the boundary crisis (to 0.00995, for instance), the system settles down onto the period-3 limit cycle and remains on it if r_{im} is then decreased back to 0.00990 (Fig. 5(B) and (D)). Thus, at $r_{\text{im}} = 0.00990$, the system can either be periodic or chaotic, depending on its past history. Of course, the transition between the strange attractor and the limit cycle can also be obtained at a fixed r_{im} value, by the perturbation of the initial conditions. The final state then depends on the location of the initial conditions with respect to the basins of attraction of the limit cycle and the strange attractor.

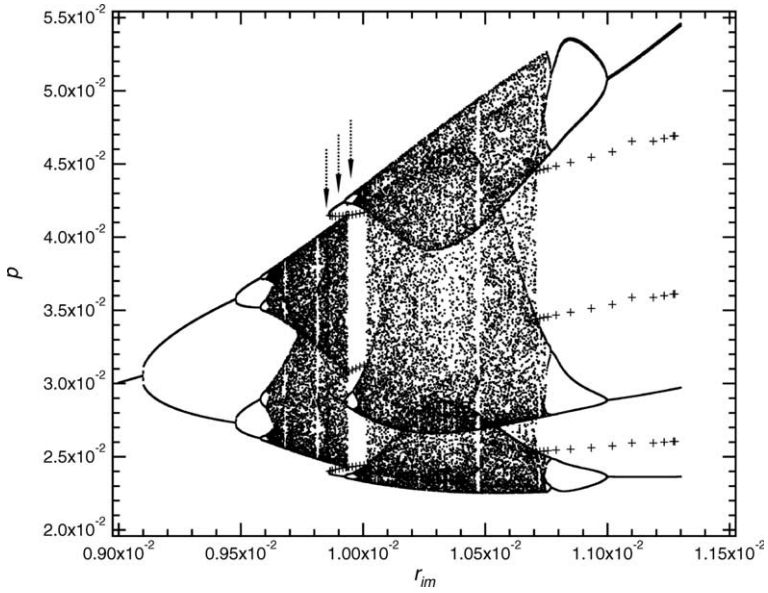

Fig. 3. Bifurcation diagram along r_{im}. The other parameters are those of Fig. 2. The plus (+) signs represent unstable orbits. The dashed arrows indicate r_{im} values of: 0.00985, 0.00990 and 0.00995.

After the boundary crisis, the stable period-3 limit cycle undergoes at its turn a cascade of period-doubling bifurcations, creating period-3×2^k limit cycles and leading to a new strange attractor. As observed for the first attractor, just after the accumulation point (Fig. 4, $r_{\mathrm{im}} = 0.0100$), first-return maps evidence period-3 noisy orbits. However in this case, the strange attractor abruptly expands at $r_{\mathrm{im}} = 0.01002$, as the unstable period-3 limit cycle derived from the saddle-node bifurcation collides inside its basin of attraction (internal crisis). The sensibility to initial conditions of this attractor is comparable to that of the first one ($\lambda_{\max} = 0.547 \pm 0.014$ bits/average orbit at $r_{\mathrm{im}} = 0.0103$). Finally, the strange attractor collapses according to the same scenario as the one that created it, but occurring now along decreasing r_{im} values. A saddle-node bifurcation occurring at $r_{\mathrm{im}} = 0.01374$ (not shown in Fig. 3) brings about an unstable and a stable period-3 limit cycle that develop along decreasing r_{im} values. The collision of the unstable orbit with the basin of attraction of the strange attractor gives rise to an internal crisis at $r_{\mathrm{im}} = 0.01068$ that greatly reduces the strange attractor. As r_{im} then increases, noisy orbits (see Fig. 4, $r_{\mathrm{im}} = 0.010715$) are replaced by stable period-3×2^k limit cycles that finally reduce, through period-halving bifurcations, to the stable period-3 limit cycle arisen from the saddle-node bifurcation at $r_{\mathrm{im}} = 0.01374$.

Many other crises inside the chaotic regions provoke alternations of chaotic and periodic dynamics. We exemplify this with the order window around $r_{\mathrm{im}} = 0.0105$ in the bifurcation diagram of Fig. 3. For $0.010465 < r_{\mathrm{im}} < 0.010480$, a stable period-12 limit cycle breaks off the chaotic dynamics. Just before the onset of this limit cycle, the dynamics evidence intermittency (Fig. 6). The system presents most of the time a periodic behavior based on the period-12 limit cycle, but from time to time (for $0.5 \times 10^6 < t < 0.9 \times 10^6$ in Fig. 6) a chaotic burst interrupts the periodic oscillations. Intermittency is due to the onset of a tangent bifurcation in the return map associated with a saddle-node bifurcation [32]. However, due to the high period of the limit cycle (period-12), the corresponding bifurcation could not be studied.

Setting $r_{\mathrm{im}} = 0.01030$, a bifurcation diagram can be obtained with β as the bifurcation parameter (Fig. 7). The diagram is qualitatively very close to that obtained with r_{im} as bifurcation parameter. A stable period-1 limit cycle arisen from a Hopf bifurcation goes to chaos through the period-doubling route. A saddle-node bifurcation occurs at $\beta = 7.459 \times 10^{-4}$, provokes a boundary crisis at $\beta = 7.468 \times 10^{-4}$, and causes bistability in between. Here again, the related stable limit cycle goes to chaos through period-doubling, expands then reduces through internal crises, and finally collapse in another (inverted) period-doubling cascade. Note that the dynamics are complex for $\beta > 7.640 \times 10^{-4}$ (not shown in Fig. 7), including another chaotic period, so that we could not identify the unstable orbit that brings about the internal crisis at $\beta = 7.557 \times 10^{-4}$. However, another kind of bistability is observed after the collapse of the strange attractor, around $\beta = 7.59 \times 10^{-4}$. Two stable period-3 limit cycles coexist and are separated by an unstable one. The "upper" stable limit cycle merges with the unstable one and disappears in a first saddle-node bifurcation at $\beta = 7.585 \times 10^{-4}$, while the "lower" one disappears through a second saddle-node bifurcation with the same unstable

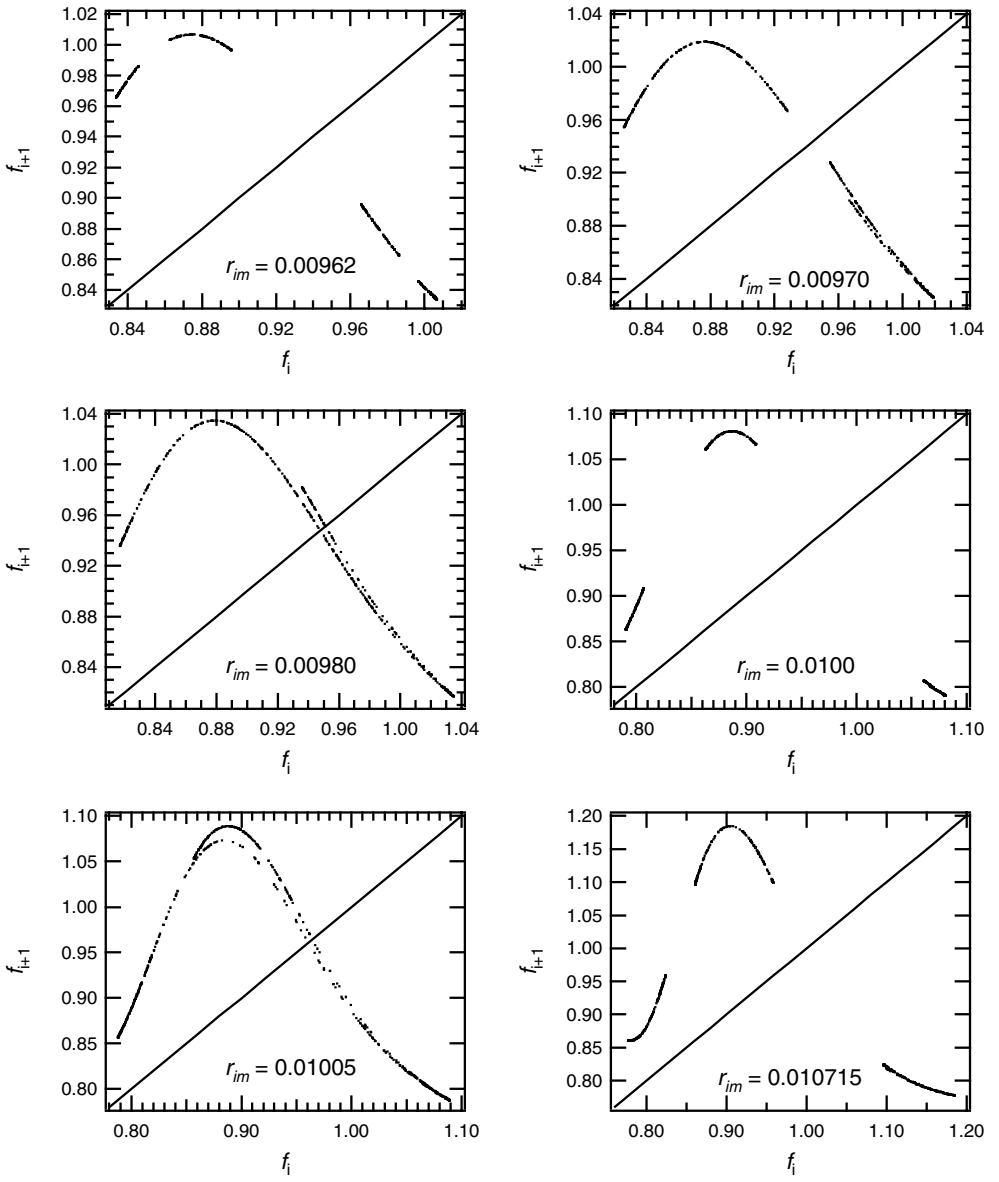

Fig. 4. First-return maps of Poincaré sections at various r_{im} values along the bifurcation diagram of Fig. 3. Poincaré sections are computed at the maxima of p.

limit cycle at $\beta = 7.592 \times 10^{-4}$. Hence, the two stable period-3 limit cycles coexist for $7.585 \times 10^{-4} < \beta < 7.592 \times 10^{-4}$. This bistable property as usual gives rise to hysteresis, as exemplified in Fig. 8: at $\beta = 7.589 \times 10^{-4}$, two different period-3 periodic oscillations are accessible to the system, depending on the initial conditions.

3.2. Higher autocatalytic levels

We exemplify the dynamics at higher autocatalytic levels with the case $\alpha = 0.2$ and $r_{im} = 0.04$. Note that for higher values, transglutaminase concentrations exceed those of the fragments in the oscillatory domains. As for low autocatalytic levels, the dynamics present an unique stable fixed point as β increases, that becomes unstable through Hopf bifurcation, leading to a period-1 limit cycle. However, the β value at the Hopf bifurcation is much higher (3.447×10^{-3}). The evolution of the system is presented as bifurcation diagram in Fig. 9, with β the bifurcation

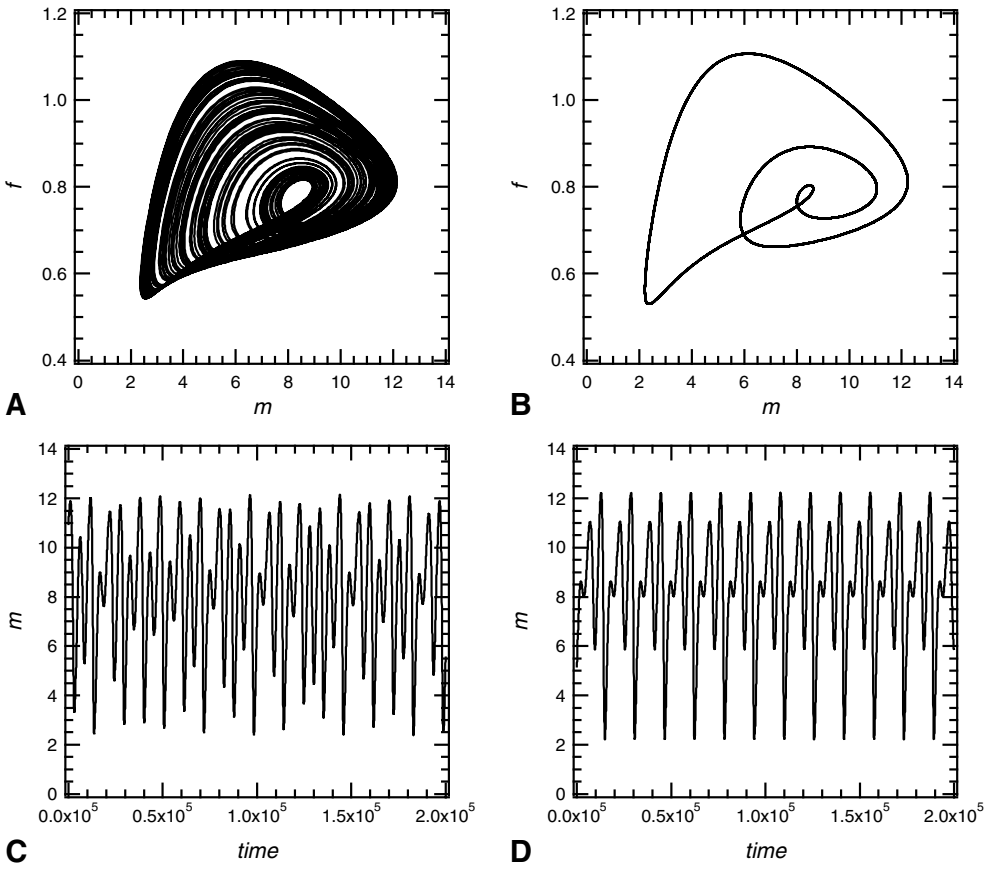

Fig. 5. Hysteresis and bistability at $r_{im} = 0.00990$ in the bifurcation diagram of Fig. 3. m–f plane projections of the trajectories (A and B) and m time evolution (C and D) obtained when r_{im} is increased from 0.00985 to 0.00990 (A and C) or decreased from 0.00995 to 0.00990 (B and D).

parameter. The first strange attractor (obtained for $0.00445 < \beta < 0.00448$) is qualitatively similar to the first attractor observed at lower autocatalytic levels (see Fig. 7, $0.000743 < \beta < 0.000747$). The sensibility to initial conditions is higher in time units ($\lambda_{max} = (5.83 \pm 0.048) \times 10^{-4}$ bits/time unit at $\beta = 004475$). However, due to its lower orbital period (circa 900 time unit), the attractor observed at high autocatalytic levels shows λ_{max} values that are similar to that observed at low autocatalytic levels, if λ_{max} is expressed with respect to one average orbit ($\lambda_{max} = 0.525 \pm 0.004$ bits/average orbit). As with low α, a saddle-node bifurcation appears at $\beta = 0.004366$, creating a stable as well as and unstable (not shown in Fig. 9) period-4 limit cycle. Nevertheless, oscillation amplitudes on the stable limit cycle are much higher at high autocatalytic levels, so that, for clarity, the bifurcation diagram of Fig. 9 presents Log(p) (rather than p) values as a function of β.

The period-4 stable limit cycle goes through one period-doubling bifurcation, but, unlike the low α case, this bifurcation does not lead to a doubling cascade. The resulting period-8 limit cycle undergoes at its turn a period-halving bifurcation so that the saddle-node bifurcation does not give rise to the second strange attractor observed with low autocatalytic levels (see Fig. 7, $0.000747 < \beta < 0.000759$). Inasmuch as the saddle-node bifurcation occurs at a β value lower than the beginning of the strange attractor, hysteresis is also observed: periodic and chaotic oscillations coexist for $0.00445 < \beta < 0.00448$. The shape of the stable limit cycle arisen from the saddle-node bifurcation is unusual, as shown in Fig. 10 for $\beta = 0.00446$. In the phase space (see the projection in the f–p plane, Fig. 10(A)) the limit cycle is tightly folded at low f and p values. The trajectories alternate between large-amplitude and small-amplitude orbits. As a result, time-variations (Fig. 10(B)) show abrupt and sharp peaks separated by periods of relative quiescence (smaller amplitude oscillations). Presumably because of these features, the unstable limit cycle born of the saddle-node bifurcation could not be traced, avoiding the identification of the crises that modify the strange attractor. However we

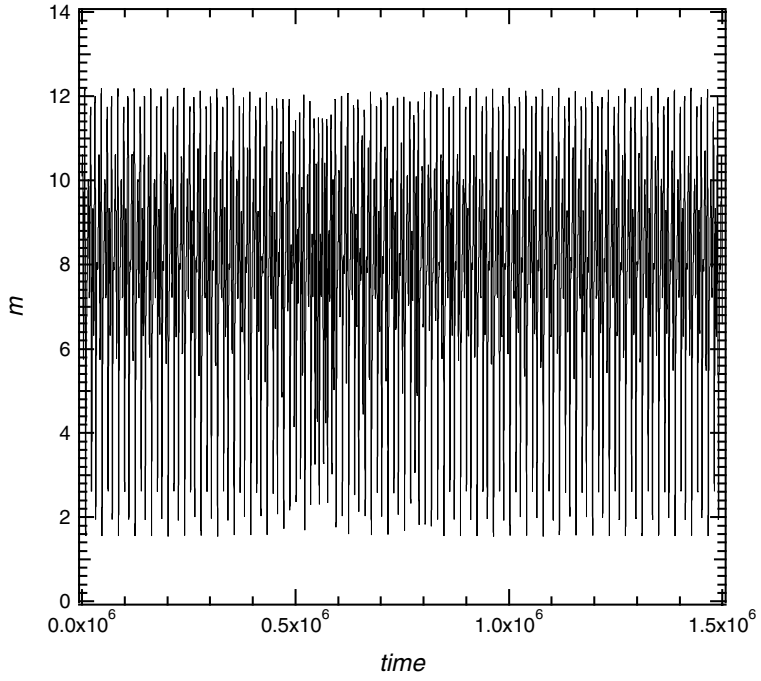

Fig. 6. Intermittency in the bifurcation diagram of Fig. 3 at $r_{im} = 0.010464$.

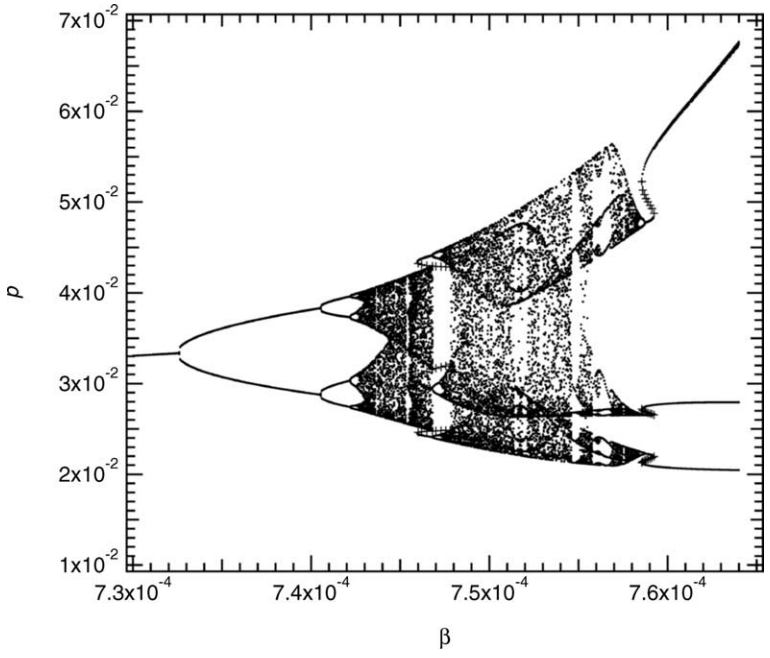

Fig. 7. Bifurcation diagram along β at $r_{im} = 0.0103$. The other parameters are those of Fig. 2. The plus (+) signs represent unstable orbits.

hypothesize its destruction at $\beta = 0.00448$ to be the result of a boundary crisis with the unstable limit cycle, as observed in the low α case.

Another chaotic zone exists at higher β values ($0.004619 < \beta < 0.004685$, Fig. 9). The corresponding strange attractor is very different from the preceding ones (Fig. 11(A)). First, it displays the same kind of abrupt peaks than the

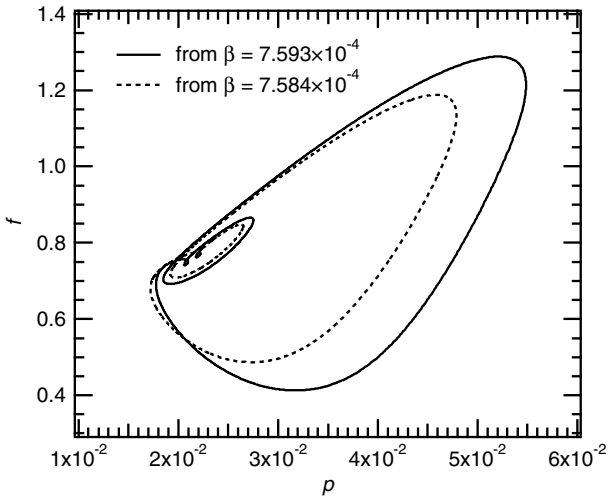

Fig. 8. Hysteresis and bistability at $\beta = 7.589 \times 10^{-4}$ in the bifurcation diagram of Fig. 7. f–p plane projections of the trajectories are obtained when β is decreased from 7.593×10^{-4} to 7.589×10^{-4} (full line) or increased from 7.584×10^{-4} to 7.589×10^{-4} (dashed line).

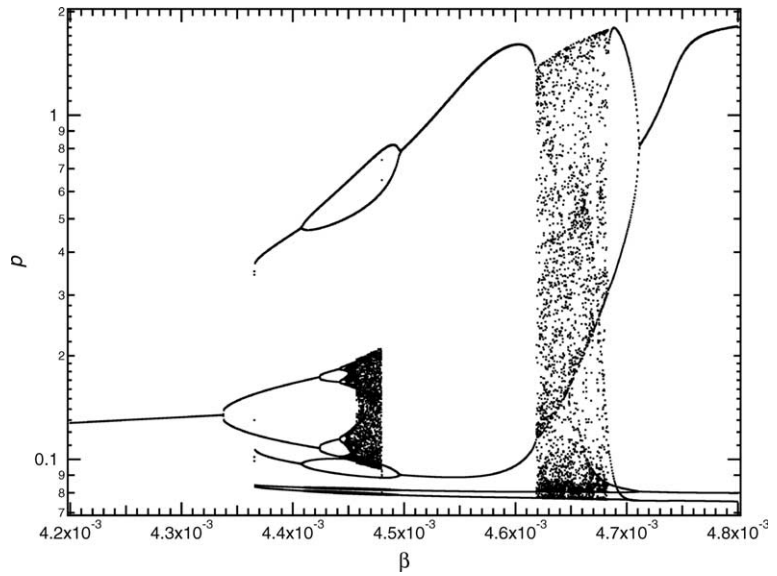

Fig. 9. Log-linear plot for the bifurcation diagram of p as a function of β for $\alpha = 0.20$ and $r_{im} = 0.040$. The other parameters are those of Fig. 2.

period-4 stable limit cycle from which it derives (Fig. 11(B)). Then, it is more sensible to initial conditions. The average orbital period varies from 3000 to 5000 time units, so that the average information loss due to chaos can be estimated between $\lambda_{max} = 1.135 \pm 0.037$ and 1.514 ± 0.061 bits/orbit at $\beta = 0.00466$ (i.e. $\lambda_{max} = (3.786 \pm 0.122) \times 10^{-4}$ bits/time units). In both cases, this value is much higher than for the Rössler system, and equivalent to that of Lorenz. Furthermore, the route towards this strange attractor is also different. Decreasing β from high values ($\beta > 0.0048$), it originates from a period-3 limit cycle that goes through a period-doubling cascade. Because of the sharpness of the peaks during the chaotic oscillations, precise determination of their maxima demand intensive calculations. Hence, Poincaré sections for this attractor were computed here at p minima (Fig. 12). Just after the period-doubling cascade (Fig. 12, $\beta = 0.004682$), first-return maps evidence period-6 noisy orbits, in agreement with the period-doubling route. The route to the strange attractor from low β values is build on the period-4 stable limit cycle, but does not consist of a period doubling cascade. Fig. 12 shows the fourth-return map of a Poincaré section for β at the limit between the

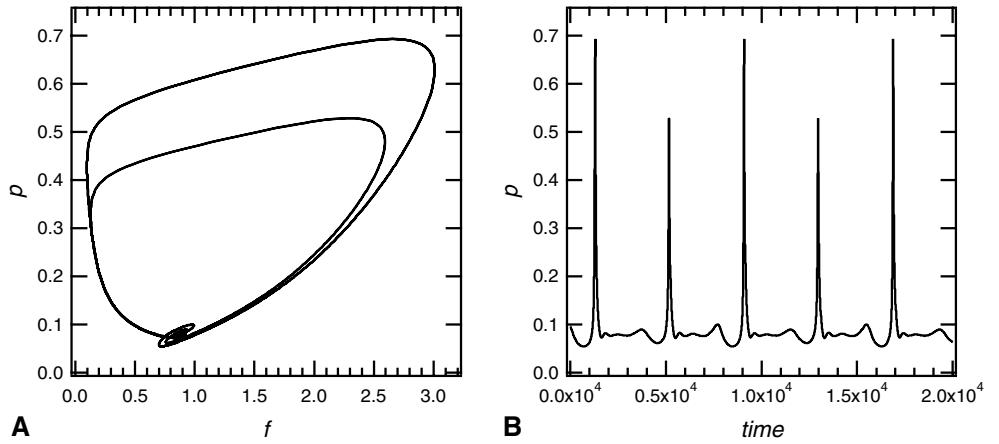

Fig. 10. (A) Projection in the p–f plane of the trajectories for $\beta = 0.00446$ ("upper" limit cycle). The other parameters are those of Fig. 9. (B) Corresponding periodic oscillations of p.

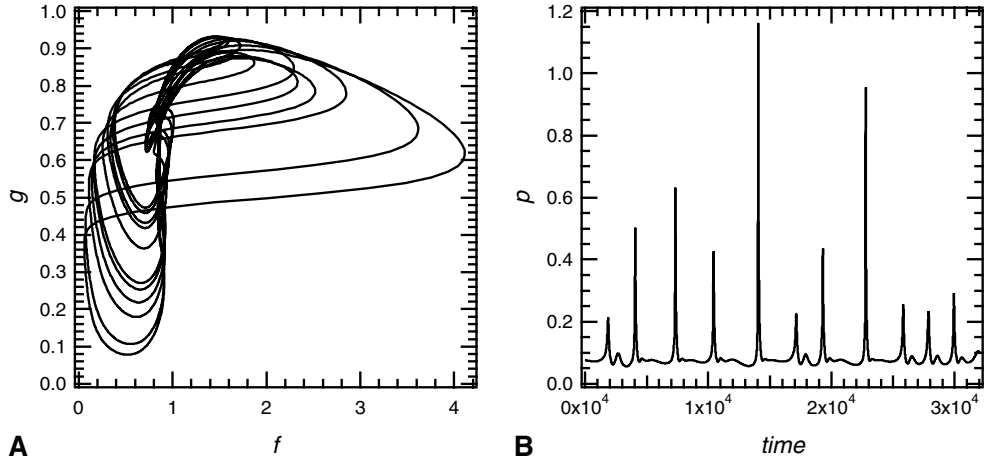

Fig. 11. (A) Projection in the g–f plane of the strange attractor for $\beta = 0.00466$ in the bifurcation diagram of Fig. 9. (B) Corresponding p time evolution. The other parameters are those of Fig. 9.

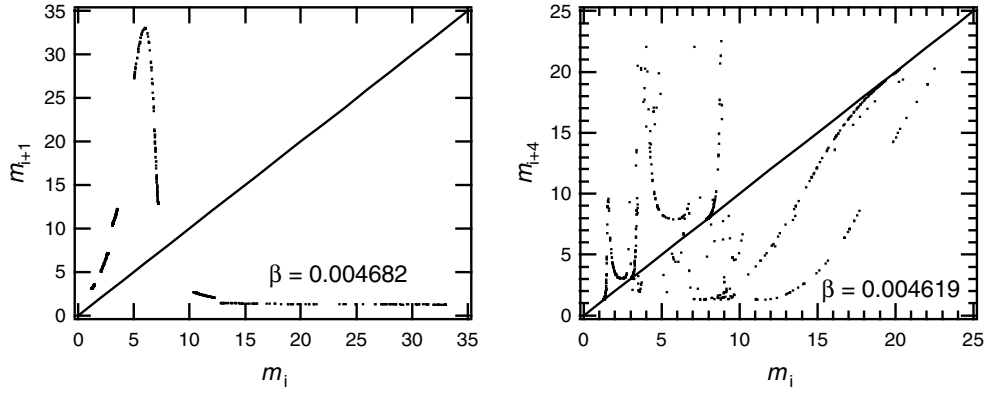

Fig. 12. First-return map at $\beta = 0.004682$ (left) and fourth-return map at $\beta = 0.004619$ (right) of Poincaré sections for the bifurcation diagram of Fig. 9. Poincaré sections are computed at the minima of p.

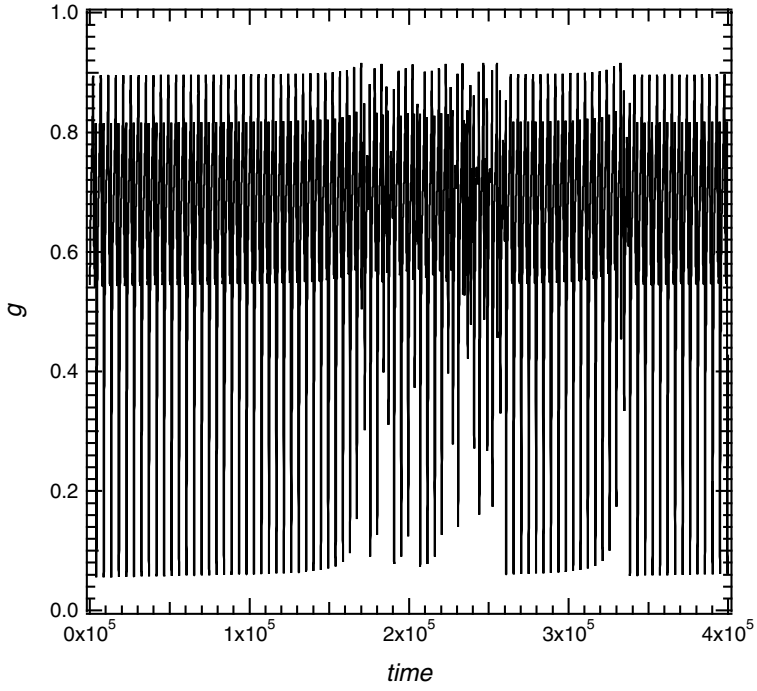

Fig. 13. Intermittency in the bifurcation diagram of Fig. 9 at $\beta = 0.004619$.

periodic and chaotic region ($\beta = 0.004619$). Although the map is very "noisy" and contains many spurious points or branches, it is clear from this figure that some branches of the map are tangent to the first diagonal. This represents a tangent bifurcation and is associated with the intermittency route to chaos [32]. In agreement with this conclusion, Fig. 13 evidences intermittency at $\beta = 0.004619$. The dynamics most of the time consist of periodic oscillations, with interruptions by a first long chaotic burst (for $1.4 \times 10^5 < t < 2.7 \times 10^5$) and another, shorter one, between $t = 3.1 \times 10^5$ and 3.4×10^5.

4. Conclusion

We have analyzed the dynamics of a bienzymatic cyclic model with two autocatalytic loops as applied to extracellular matrix turnover. When the influences of the loops are low, the system presents limit-cycle oscillations that give rise to successive chaotic behaviors through period-doubling cascades. The succession of the corresponding strange attractors is dictated by boundary and internal crisis. With higher autocatalytic levels, one of the strange attractor is lost, because the corresponding period-doubling cascade does not occur, while another strange attractor arises through intermittency. In both case, the system displays bistability properties, when a limit cycle coexists with another one or with a strange attractor.

Complex or chaotic dynamics have previously been observed in a number of biological models. Although the most abundant literature concerns population (ecological) models (see, for example, [33–35] for recent studies), models for all biological organization scales have also evidenced chaotic behaviors, including physiology [36–38] and biochemistry [39–41]. However, while evidenced during in vitro laboratory experiments [42–44], univocal proofs of chaotic behaviors in real biological systems are still missing. Despite this uncertainty, chaotic dynamics are attractive to biologists, because they could provide biological systems with a wide richness of behaviors to explain biological oscillations and rhythms [45,46].

Decroly and Goldbeter [47] studied a biochemical model that is closely related to our model. They addressed the dynamics of two allosteric enzymes activated by their respective product and coupled in series. The main difference with our model lies in its linear arrangement which is replaced in our case by a cyclic organization. Furthermore, the two autocatalytic loops originate in our model from enzyme synthesis by the cells, not from direct regulation of the enzyme activity by the reaction products. However, both models exhibit complex oscillatory behaviors, including chaos and bi-

(or multi-)stability properties, although each one presents specific characteristic. For instance, we did not find the bursting dynamics (spike-like oscillations separated by periods of moderate variations) that arise in Decroly and Goldbeter's model via the coupling of two oscillatory mechanisms of different time-scales.

In our model, complex behaviors appear only if the autocatalytic loops thresholds are different, namely if $K_R > K_S$. If this condition is not fulfilled, the system only presents stable steady-states. One explanation could possibly reside in the highly nonlinear characteristics of the system in the case $K_R > K_S$. Indeed, in this case, the $k_p r_p / k_g r_g$ ratio (representing the ratio between both enzyme activity synthesis by the cells) is almost constant up to $f \approx K_S$ and increases nonlinearly for higher f concentrations. Hence, whenever $f > K_S$, fragments indirectly amplify their own increase. For $K_R \leqslant K_S$, the $k_p r_p / k_g r_g$ ratio decreases when $f > K_S$, and f variations are damped by the system.

Our previous study suggested the possibility of periodic oscillations during extracellular matrix turnover [14]. The present paper shows that the presence of a second autocatalytic loop could greatly enlarge the variety of the oscillatory behaviors, including smooth or sharp, periodic or chaotic evolutions, as well as bistable areas between some of these behaviors. However, this greater variety comes with a substantial increase of the average period. In the present paper, (average) orbital periods range from 900 to 5×10^3 dimensionless time units. This roughly corresponds to periods of the order of 10 h (with k_p ranging from 50 to 500/h [48]), whereas oscillation periods with a single autocatalytic loop fall in the range of minutes. Hence, experimental testing of the theoretical results should be accessible to conventional cellular biology methods.

References

[1] Goldbeter A, Koshland DE. Sensitivity amplification in biochemical systems. Q Rev Biophys 1982;15:555–91.
[2] Ferrell JE. Tripping the switch fantastic: how a protein kinase cascade can convert graded inputs into switch-like outputs. Trends Biochem Sci 1996;21:460–6.
[3] Ferrell JE, Machleder EM. The biochemical basis of an all-or-none cell fate switch in *Xenopus* oocytes. Science 1998;280:895–8.
[4] Lisman JE. A mechanism for memory storage insensitive to molecular turnover: A bistable autophosphorylating kinase. Proc Natl Acad Sci USA 1985;82:3055–7.
[5] Hervagault JF, Canu S. Bistability and irreversible transitions in a simple substrate cycle. J Theor Biol 1987;127:439–49.
[6] Guidi GM, Goldbeter A. From bistability to oscillations in a model for the isocitrate dehydrogenase reaction. Biophys Chem 1998;71:201–10.
[7] Guidi GM, Goldbeter A. Oscillations and bistability predicted by a model for a cyclical bienzymatic system involving the regulated isocitrate dehydrogenase reaction. Biophys Chem 2000;83:153–70.
[8] Zhabotinsky AM. Bistability in the Ca^{2+}/Calmodulin-dependent protein kinase-phosphatase system. Biophys J 2000;79:2211–21.
[9] Ferrell JE, Xiong W. Bistability in cell signaling: how to make continuous processes discontinuous and reversible processes irreversible. Chaos, Solitons & Fractals 2001;11:227–36.
[10] Gonze D, Goldbeter A. A model for a network of phosphorylation–dephosphorylation cycles displaying the dynamics of dominoes and clocks. J Theor Biol 2000;210:167–86.
[11] Schellenberger W, Hervagault JF. Irreversible transitions in the 6-phosphofructokinase/fructose 1,6-bisphosphatase cycle. Eur J Biochem 1991;195:109–13.
[12] Coevoet MA, Hervagault JF. Irreversible metabolic transitions: the glucose 6-phosphate metabolism in yeast cell-free extracts. Biochem Biophys Res Commun 1997;234:162–6.
[13] Guidi GM, Carlier MF, Goldbeter A. Bistability in the isocitrate dehydrogenase reaction: an experimentally based theoretical study. Biophys J 1998;74:1229–40.
[14] Larreta-Garde V, Berry H. Modeling extracellular matrix degradation balance with proteinase/transglutaminase cycle. J Theor Biol 2002;217:105–24.
[15] Hay ED. Cell biology of extracellular matrix. New York: Plenum Press; 1981.
[16] Basbaum CB, Werb Z. Focalized proteolysis: spatial and temporal regulation of extracellular matrix degradation at the cell surface. Curr Opin Cell Biol 1996;8:731–8.
[17] Price JT, Bonovich MT, Kohn EC. The biochemistry of cancer dissemination. Crit Rev Biochem Mol 1997;32:175–253.
[18] Perris R, Perissinotto D. Role of the extracellular matrix during crest cell migration. Mech Dev 2000;95:3–21.
[19] Dustin ML, de Fougerolles AR. Reprograming T cells: the role of extracellular matrix in coordination of T cell activation and migration. Curr Opin Immunol 2001;13:286–90.
[20] Hulboy DL, Rudolph LA, Matrisian LM. Matrix metalloproteinases as mediators of reproductive function. Mol Human Reprod 1997;3:27–45.
[21] Witte MB, Barbul A. General principles of wound healing. Surg Clin North Am 1997;77:509–28.
[22] Liotta LA, Steeg PS, Stetler-Stevenson WG. Cancer metastasis and angiogenesis: An imbalance of positive and negative regulation. Cell 1997;64:327–36.
[23] LaFlamme SE, Auer KL. Integrin signaling. Seminars Cancer Biol 1996;7:111–8.
[24] Yamada KM. Integrin signaling. Matrix Biol 1997;16:137–41.

[25] Werb Z, Tremble PM, Behrendtsen O, Crowley E, Damsky C. Signal transduction through the fibronectin receptor induces collagenase and stromelysin gene expression. J Cell Biol 1989;109:877–89.
[26] Haroon ZA, Lai TS, Hettasch JM, Lindberg RM, Dewhirst MW, Greenberg CS. Tissue transglutaminase is expressed as a host response to tumor invasion and inhibits tumor growth. Lab Invest 1999;79:1679–86.
[27] Segel IH. Enzyme kinetics. New-York: Wiley Interscience; 1993. p. 18–99.
[28] Segel LA, Slemrod M. The quasi-steady state assumption: a case study in perturbation. SIAM Rev 1989;3:466–77.
[29] Wolf A, Swift JB, Swinney HL, Vastano JA. Determining Lyapunov exponents from a time series. Physica D 1985;16:285–317.
[30] Gilmore R. Topological analysis of chaotic dynamical systems. Rev Mod Phys 1998;70:1455–529.
[31] Grebogi C, Ott E, Yorke JA. Crises, sudden changes in chaotic attractors and chaotic transients. Physica D 1983;7:181–200.
[32] Pomeau Y, Manneville P. Intermittent transition to turbulence in dissipative dynamical systems. Commun Math Phys 1980;74:189–97.
[33] Letellier C, Aziz-Alaoui MA. Analysis of the dynamics of a realistic ecological model. Chaos, Solitons & Fractals 2002;13:95–107.
[34] Cushing M, Henson SM, Desharnais RA, Dennis B, Costantino RF, King A. A chaotic attractor in ecology: theory and experimental data. Chaos, Solitons & Fractals 2001;12:219–34.
[35] Vandermeer J, Stone L, Blasius B. Categories of chaos and fractal basin boundaries in forced predator-prey models. Chaos, Solitons & Fractals 2001;12:265–76.
[36] Wang L, Pichler EE, Ross J. Oscillations and chaos in neural networks: an exactly solvable model. Proc Natl Acad Sci USA 1990;87:9467–71.
[37] Cai D, Lai Y, Winslow RL. Complex dynamics in coupled cardiac pacemaker cells. Phys Rev Lett 1993;71:2501–4.
[38] Goldberger AL, Amaral LA, Hausdorff JM, Ivanov PCh, Peng CK, Stanley HE. Fractal dynamics in physiology: alterations with disease and aging. Proc Natl Acad Sci USA 2002;99(Suppl 1):2466–72.
[39] Bronnikova TV, Schaffer WM, Hauser MJB, Olsen LF. Routes to chaos in the peroxidase-oxidase reaction. 2. The fat torus scenario. J Phys Chem B 1998;102:632–40.
[40] Kaern M, Hunding A. The effect of slow allosteric transitions in a coupled biochemical oscillator model. J Theor Biol 1999;198:269–81.
[41] Romond PC, Rustici M, Gonze D, Goldbeter A. Alternating oscillations and chaos in a model of two coupled biochemical oscillators driving successive phases of the cell cycle. Ann N-Y Acad Sci 1999;879:180–93.
[42] Schiff SJ, Jerger K, Duong DH, Chang T, Spano ML, Ditto WL. Controlling chaos in the brain. Nature 1994;370:615–20.
[43] Costantino RF, Desharnais RA, Cushing JM, Dennis B. Chaotic dynamics in an insect population. Science 1997;275:389–91.
[44] Nielsen K, Sorensen PG, Hynne F. Chaos in glycolysis. J Theor Biol 1997;186:303–6.
[45] Goldberger AL. Is the normal heartbeat chaotic or homeostatic? News Physiol Sci 1991;6:87–91.
[46] Goldbeter A. Biochemical oscillations and biological rythms. The molecular basis of periodic and chaotic behaviour. Cambridge: Cambridge University Press; 1996.
[47] Decroly O, Goldbeter A. From simple to complex oscillatory behaviour: Analysis of bursting in a multiply regulated biochemical system. J Theor Biol 1987;124:219–50;
Decroly O, Goldbeter A. Birhythmicity, chaos, and other patterns of temporal self-organization in a multiply regulated biochemical system. Proc Natl Acad Sci USA 1982;79:6917–22.
[48] Birkedal-Hansen H, Moore WGI, Bodden MK, Windsor LJ, Birkedal-Hansen B, DeCarlo A, et al. Matrix metalloproteinases: a review. Crit Rev Oral Biol 1993;4:197–250.